Basic and charge density wave modulated structures of NbS_3-II

E. Zupanič,[1,*] H. J. P. van Midden,[1] M. A. van Midden,[1] S. Šturm,[1] E. Tchernychova,[2] V. Ya. Pokrovskii,[3,†] S. G. Zybtsev,[3] V. F. Nasretdinova,[3] S. V. Zaitsev-Zotov,[3] W. T. Chen,[4] Woei Wu Pai,[4,5,‡] J. C. Bennett,[6] and A. Prodan[1]

[1]*Jožef Stefan Institute, Jamova 39, SI-1000 Ljubljana, Slovenia*

[2]*Department of Materials Chemistry, National Institute of Chemistry, Hajdrihova 19, SI-1000 Ljubljana, Slovenia*

[3]*Kotel'nikov Institute of Radioengineering and Electronics of Russian Academy of Sciences (RAS), Mokhovaya 11-7, 125009 Moscow, Russia*

[4]*Center for Condensed Matter Sciences, National Taiwan University, Taipei 106, Taiwan*

[5]*Department of Physics, National Taiwan University, Taipei 106, Taiwan*

[6]*Department of Physics, Acadia University, Wolfville, Nova Scotia, Canada B4P 2R6*

(Received 7 May 2018; revised manuscript received 31 August 2018; published 27 November 2018)

The basic and the charge density wave (CDW) structures of the monoclinic NbS_3-II polymorph were studied by synchrotron x-ray diffraction, *ab initio* calculations, simulation of electron diffraction patterns, and by atomic-resolution transmission electron and low-temperature scanning tunneling microscopies. It is confirmed that the basic structure belongs to the space group $P2_1/m$ and is described with a unit cell, formed of four pairs of symmetry-related trigonal prismatic (TP) columns [$a_0 = 0.96509(8)$ nm, $b_0 = 0.33459(2)$ nm, $c_0 = 1.9850(1)$ nm, and $\beta_0 = 110.695(4)^\circ$]. The incommensurate components of the two CDWs, $\vec{q}_1 = (0,\ 0.298,\ 0)$ and $\vec{q}_2 = (0,\ 0.352,\ 0)$, are related as $q_{1_b} + 2q_{2_b} \approx 1$. Both CDWs form their own modulation patterns with unit cells ($a_m = 2a_0$, $b_m = b_0/q_{jb}$, $c_m = c_0$, $\beta_m = \beta_0$) and are ordered along adjacent isosceles TP columns either pairwise or with both columns modulated by either the $\vec{q}_1$ or $\vec{q}_2$ CDW only. The CDWs are ordered according to one of the two possible modulation pattern space groups, Cm or $C2/m$. If considered as long-period commensurate, the entire modulated structure with both CDWs included is described within experimental error with an enlarged unit cell ($a = 2a_0$, $b = 37b_0$, $c = c_0$, and $\beta = \beta_0$) and with all atoms displaced from their average positions in accord with the specified modulation pattern.

DOI: 10.1103/PhysRevB.98.174113

I. INTRODUCTION

A large number of quasi-one-dimensional (1D) transition-metal trichalcogenides (MX_3), which all possess related structures [1,2], are now known. They are composed of bi-caped trigonal prismatic (TP) columns, formed of chalcogen atoms and centered by metallic chains. The metal atoms are additionally linked to the chalcogen atoms of the neighboring columns, becoming thus eight-coordinated. The 1D columns are alternately shifted in phase by half the unit cell height and are strongly bonded into layers, separated by relatively wide Van der Waals (VdW) gaps. As a result, the structures show a strong 1D as well as a two-dimensional (2D) character with very anisotropic structural and transport properties.

Depending on the growth conditions, NbS_3 single crystals present a variety of polymorphs [3]. However, only two of these (NbS_3-I and NbS_3-II) have been studied in detail [2]. The structure of NbS_3-I was solved long ago [4] and was characterized by a pronounced dimerization along its triclinic $\vec{b}_0$ axis. In contrast to NbS_3-I single crystals, whose dimensions are usually sufficiently large to enable conventional single-crystal x-ray structural analysis, single crystals of NbS_3-II are typically much smaller and have a less pronounced 2D character. The hairlike morphology, small size and tendency to bend of NbS_3-II crystals, coupled with a slight nonstoichiometry of about 3% S deficiency, as measured by electron probe microanalysis (EPMA) [5], has prevented the basic and the CDW-modulated structures of NbS_3-II from being accurately determined by means of single-crystal x-ray analysis. It was, however, clearly shown in electron diffraction experiments that in the case of NbS_3-II, weak pairs of satellites, whose incommensurate (IC) components appear close to $\approx\frac{1}{3}b_0^*$ in the corresponding diffraction patterns (DP) [6,7], replace the characteristic dimerization in NbS_3-I. The superstructure of the NbS_3-I polytype was also alternatively described by means of the two-line superspace group (SSG) notation, mainly developed for a description of the IC modulated structures in a $3+1$-dimensional superspace [8,9], as $P\,{}^{P2_1/m}_{1\ \bar{1}}(0\ \beta\ 0)$ with $\beta = 0.5$ [10]. The same SSG two-line notation was also determined from electron DPs for the description of the IC modulated structure of NbS_3-II, as $A\,{}^{P2_1/m}_{1\ \bar{1}}$ (No. $11b.6.1$) [11] and by means of the corresponding dualistic notation [12] as ${}^{mP2_1/m}_{cB2/m}$ (both with interchanged axes with regard to the present description, i.e., with $\vec{c}_0$ being the direction of the IC modulation). Since many interesting and unique physical properties of NbS_3-II have been reported and summarized [5], it is imperative to determine the basic structure of NbS_3-II and a plausible model of the complicated CDW modulated structure.

The unique structure-dependent physical properties of NbS_3-II, including the observation of a third independent CDW-driven phase transition [5], have rendered the

*erik.zupanic@ijs.si
†pok@cplire.ru
‡wpai@ntu.edu.tw

identification of the heretofore unknown basic structure a problem of significance. As for a few other MX_3 compounds, e.g., $NbSe_3$ and the monoclinic polymorph of TaS_3 (m-TaS_3) [13,14], pairs of IC satellites in the electron DPs of NbS_3-II [6] correspond to two CDWs with satellites at position (0.5, 0.298, 0) and (0.5, 0.352, 0) [2,15,16]. The nonzero x parameters (0.5) of these positions are in fact a result of the extinction rules, imposed by the modulation pattern space group (G_M) [17], while the actual modulation of both CDWs is directed along the columns with $\vec{q}_1 = (0,\ 0.298, 0)$ and $\vec{q}_2 = (0,\ 0.352,\ 0)$. The two CDWs show different onset temperatures ($\vec{q}_1$ at $T_1 \approx 360$K and $\vec{q}_2$ at $T_2 \approx 460$ K [18]) and were shown to slide under an external electric field [19]. A further interesting similarity between NbS_3-II and $NbSe_3$ is the fact that the two $\vec{q}$ vectors are in both cases obviously related, with their IC components adding into a commensurate (COM) value within experimental error. If the structure is considered as a long-period (LP) COM, the two IC CDWs in NbS_3-II fit closely to 5 and 6 modulation periods per $17b_0$ [6] and add closely to a COM value as $q_{1_b} + q_{2_b} \approx 2/3$ [6]. However, the situation in NbS_3-II is further complicated in comparison to $NbSe_3$. In addition to the two aforementioned CDWs, which both show clear evidence of the structural modulation in electron DPs, a third CDW is detected in transport measurements, with an onset temperature of about 150 K [19]. In contrast to the two previously identified CDWs, this third CDW shows a very low and vastly varied concentration of carriers (between 3 and 1000 times lower than that of $\vec{q}_2$) and practically no evidence of its existence in the corresponding structural studies [20]. Another complication in case of NbS_3-II is its appearance in two subphases, high- and low-ohmic samples [19] with different electrical conductivities and possibly a slight difference in stoichiometries. Only the low-ohmic subphase shows the 150 K transition.

The present study was undertaken in order to acquire a better understanding of the basic and the modulated structures of NbS_3-II. Synchrotron x-ray powder diffraction (XRD), high-resolution (HR) scanning transmission electron (STEM) and scanning tunneling microscopy (STM) studies were performed in conjunction with *ab initio* calculations of the basic structure, in relation to the known structures of NbS_3-I and $NbSe_3$. The experimental and calculated electron diffraction patterns are also compared to restrict the plausible modulated CDW structures.

The employment of a broad range of complementary techniques has finally allowed a refinement of the NbS_3-II basic structure. In addition, the structures of both IC CDW modulation patterns are proposed and related to the basic structure. The details of the entire modulated structure, modeled as LP COM, are also provided.

II. EXPERIMENTAL

The NbS_3-II whiskers were grown in a three-zone furnace with separate temperature control for each zone with typical set temperatures of 750 °C, 700 °C, and 650 °C [19]. HR STEM images were acquired with an aberration-corrected probe in a TEM (JEOL JEM-ARM200F), using a cold field emission source. The probe size was 0.1 nm, with a current of 20 pA and a convergence semiangle of 24 mrad. The collection semiangle for the high-angle annular dark-field (HAADF) detector was set between 45 and 180 mrad. A Wiener filter was applied on high-resolution experimental images to improve the visibility of the crystalline matrix in the presence of partially amorphous surface layers [21]. The HAADF-STEM images were calculated using the QSTEM code [22] by applying the same electron-optical parameters as used during the experimental image acquisition. Finally, the Poisson noise was added onto the calculated images to mimic the background noise of the HAADF detector.

STM was conducted on an Omicron low-temperature (LT) STM, operated between 78 and 160 K, with a base pressure of 2.5×10^{-11} Torr. Flashed tungsten tips were used. The NbS_3-II whisker samples were freshly cleaved *in situ* in ultrahigh vacuum at room temperature.

XRD experiments were conducted for phase identification and for structural analysis. The XRD patterns were recorded with a Rayonix MX225HE CCD detector and a beam energy of 18 keV at the beamline BL12B2, Spring-8 (Japan), and with a MYTHEN detector and a beam energy of 15 keV at the beamline 09A, Taiwan Photon Source (TPS), National Synchrotron Radiation Research Center (Taiwan). The fine NbS_3-II whiskers were carefully and repeatedly cut by razor blades and packed into 0.3-mm borosilicate capillaries. The capillary was kept spinning during data collection for powder averaging. The diffraction patterns were analyzed with the Le Bail and Rietveld methods using the Bruker DIFFRAC.TOPAS [23] program. Since the Spring-8 and TPS data gave similar results, only the Spring-8 data are presented.

Density functional theory (DFT) calculations were performed using the QUANTUM ESPRESSO code [24]. In this approach, the electron-ion interactions are described by the Garrity-Bennett-Rabe-Vanderbilt (GBRV) high throughput ultrasoft pseudopotentials [25], with the generalized gradient approximation of the exchange and correlation functional of Perdew, Burke, and Ernzerhof (PBE) [26]. For the plane-wave basis set expansion, the kinetic cutoff energy was at 40 Ry. Based on the size of the simulation cell, either a (4,4,2) or a (2,4,2) Monckhorst-Pack k-point sampling grid was used. The atomic structure was relaxed until the changes in total energy were below 1.0×10^{-6} Ry and the forces below 1.0×10^{-5} atomic units.

III. RESULTS

A main result is the successful refinement of the NbS_3-II basic structure, as shown in Fig. 1. Its unit cell is composed of four symmetry-related pairs of TP columns, three isosceles and one almost equilateral, which clearly resembles the structure of $NbSe_3$. The corresponding structural data are collected in Table I.

In addition, the structures of both IC CDW modulation patterns are proposed and related to the basic structure. The structural details of both CDWs are shown in Fig. 6 and summarized in Table II, while the details of the entire modulated structure, considered as LP COM, are given in Table III.

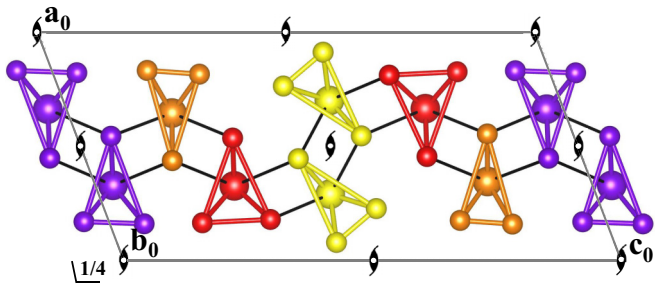

FIG. 1. The basic structure of NbS_3-II [$a_0 = 0.96509(8)$ nm, $b_0 = 0.33459(2)$ nm, $c_0 = 1.9850(1)$ nm, and $\beta_0 = 110.695(4)^\circ$]. Large balls represent Nb and the small ones S atoms. There are four symmetry-related pairs of TP columns in the unit cell, three isosceles (Y, O, and P) and one almost equilateral (R). The two inter-column Nb-S bonds of the eight bonds forming the bi-capped trigonal prisms are shown in black. The symmetry elements of the space group $P2_1/m$ are added.

A. Le Bail x-ray powder diffraction analysis

In comparison with XRD characterization using the Bragg-Brentano geometry, a significant improvement of diffraction profiles was achieved with synchrotron XRD. The Le Bail method was first applied to compare the experimental powder x-ray diagrams with several suggested unit-cell parameters [4,11,27–29]. Best fit was obtained with the parameters of Van Smaalen [29], $a_0 = 0.9650$ nm, $b_0 = 0.3345$ nm, $c_0 = 1.8749$ nm, $\beta_0 = 98.07^\circ$, and space group $P2_1/m$. However, we decided to use a transformed cell with $a_0 = 0.9654$ nm, $b_0 = 0.3346$ nm, $c_0 = 1.9855$ nm, and $\beta_0 = 110.71^\circ$ in this work. These two unit cells have identical cell volumes and the XRD patterns are equally well fitted with either of them. The transformed unit cell was chosen not only because the modified structure parameters clearly resemble that of $NbSe_3$ [13,15] but also because the two axes ($\vec{b}_0$ and $\vec{c}_0$) are chosen to be parallel to the VdW gaps. This offers a more straightforward characterization of the HR STEM and LT STM images as well as the corresponding electron DPs.

TABLE I. Structural parameters of the basic structure of NbS_3-II, obtained by *ab initio* calculation and improved by the Rietveld refinement of a synchrotron XRD pattern. O, R, Y, and P refer to orange, red, yellow, and purple columns, respectively.

$a_0 = 0.96509(8)$ nm, $b_0 = 0.33459(2)$ nm, $c_0 = 1.9850(1)$ nm
$\beta_0 = 110.695(4)^\circ$, Rwp = 5.75%, GOF = 2.68
Space group $P2_1/m$ (No. 11)
Nb and S atoms in 2*e* special positions

Atom	Column	x_0	y_0	z_0
Nb	Y	0.7005(8)	0.75000	0.5280(3)
S	Y	0.546(2)	0.25000	0.5767(9)
S	Y	0.913(2)	0.25000	0.5490(8)
S	Y	0.740(2)	0.25000	0.4422(9)
Nb	R	0.6893(9)	0.25000	0.7217(3)
S	R	0.840(2)	0.75000	0.8071(9)
S	R	0.828(2)	0.75000	0.6751(9)
S	R	0.469(2)	0.75000	0.681(1)
Nb	O	0.368(1)	0.75000	0.7876(4)
S	O	0.178(2)	0.25000	0.7946(9)
S	O	0.204(2)	0.25000	0.697(1)
S	O	0.579(2)	0.25000	0.8297(9)
Nb	P	0.662(1)	0.25000	0.9675(4)
S	P	0.835(3)	0.75000	0.056(1)
S	P	0.842(2)	0.75000	0.9461(9)
S	P	0.446(3)	0.75000	0.930(1)

TABLE II. The structural parameters of the $\vec{q}_1$ and $\vec{q}_2$ CDW modulation patterns for one of two possible arrangements. The alternate arrangement is obtained by interchanging $\vec{q}_1$ and $\vec{q}_2$ on O and P columns. The modulation pattern unit cell with only one CDW present is obtained by replacing all $\vec{q}_1$ values with the $\vec{q}_2$ ones, which increases the symmetry into $C2/m$ (No. 12). O and P refer to orange and purple, respectively.

$a_m = 2a_0$, $b_m = b_0/q_{jb}$ ($j = 1, 2$), $c_m = c_0$, $\beta_m = \beta_0$
Space group Cm (No. 8)
Both CDWs related as 2*a* special positions

CDW	column	x_m	x_m	x_m
$\vec{q}_1$	O	0.17485	0.00000	0.79057
$\vec{q}_1$	P	0.16619	0.00000	0.03656
$\vec{q}_2$	O	0.32515	0.50000	0.20943
$\vec{q}_2$	P	0.33381	0.50000	0.96344

B. Atomic-resolution high-angle angular dark-field scanning transmission electron microscopy

Figure 2(a) shows a raw and a processed HAADF-STEM image of NbS_3-II with the beam aligned along the [001] zone axis. An inset of a simulated image based on the proposed structural model, determined by combining experimental (XRD, HR STEM, and LT STM) and theoretical (*ab initio* calculations) studies, is shown overlaid on the processed experimental image. A fast Fourier transform (FFT) of the experimental image is shown in the upper right inset, with only the $\vec{q}_2$ IC satellites clearly resolved in this instance. It is consistently observed that the satellites, whether present as complete doublets or as $\vec{q}_2$ singlets, appear relatively sharp only in the shown [001] zone axis patterns. By tilting the sample from the [001] toward the [100] zone around the $\vec{b}_0$ axis, the satellites in the DPs become progressively weaker and elongated to form streaks connecting the IC satellites perpendicular to the $\vec{b}_0^*$ direction. These streaks become essentially undetectable in the [100] zone axis pattern. Consequently, the HR STEM images, recorded with the beam along the NbS_3-II [100] zone axis, are generally of poor quality in comparison with those recorded along the [001] crystal zone. The streaking in the DPs arises from the presence of numerous defects, clearly detected along the $\vec{c}_0$ direction in STM images of the (100) VdW surfaces. The HR STEM images with the corresponding DPs and FFTs, recorded along the [100] zone axis, are therefore useless for structural modeling.

After FFT filtering and inverse FFT (IFFT) of the Fig. 2(a), evidence of the IC CDW modulation is clearly observed, as shown in Fig. 2(b). Most often only the stronger ($\vec{q}_2$) of the two satellites forming a pair is detected in the DPs and the FFTs. The second satellite ($\vec{q}_1$) is always much weaker or even absent at room temperature [6,11] (as is the case in the

TABLE III. The structural parameters of the NbS_3-II overall modulated structure with both, $\vec{q}_1$ and $\vec{q}_2$ modes present, and for the two cases considered ($n = 36,\ 37$ and with m ranging from 0 to n-1). Only one of two possible arrangements is given. The alternate possibility is obtained by interchanging all P1 and P2, $P1 = 11\,2^{\cdot}$ and $P2 = 13\,2^{\cdot}$ for the two values of n, respectively. In case all O and P columns are modulated by $\vec{q}_2$ modes only, all P1 values are to be replaced by the P2 values, which increases the symmetry into $P\bar{1}$ (No. 2). P1 and P2 stay for $\vec{q}_1$ and $\vec{q}_2$ modes, O and P refer to orange and purple columns, and the subscripts +c and −c to + cos and − cos functions, respectively.

$a = 2a_0$, $b = nb_0$ ($n = 36, 37$), $c = c_0$, $\beta = \beta_0$, Space group $P1$ (No. 1)
All atoms in general 1a positions; all Nb atoms and the S atoms of R and Y columns in unmodulated positions given in Table I and the remaining S atoms of O and P columns displaced according to the following modulation scheme:

Atom	Column	x	y	z
S	O(1/−c)	0.089100 (−A(−0.69974) cos[(m/n + 1/(4n)) P1])	[m/n+1/(4n)]	0.79469 (−A(0.71440) cos[(m/n + 1/(4n)) P1])
S	O(1/−c)	0.10210 (−A(−0.82646) cos[(m/n + 1/(4n)) P1])	[m/n+1/(4n)]	0.69710 (−A(0.56299) cos[(m/n + 1/(4n)) P1])
S	O(1/−c)	0.28960 (−A(−0.19717) cos[(m/n + 1/(4n)) P1])	[m/n+1/(4n)]	0.82979 (−A(0.98037) cos[(m/n + 1/(4n)) P1])
S	P(2/+c)	0.41765 (+A(0.10895) cos[(m/n + 3/(4n)) P2])	[m/n+3/(4n)]	0.056100 (+A(−0.99405) cos[(m/n + 3/(4n)) P2])
S	P(2/+c)	0.42110 (+A(0.32224) cos[(m/n + 3/(4n)) P2])	[m/n+3/(4n)]	0.94619 (+A(0.94666) cos[(m/n + 3/(4n)) P2])
S	P(2/+c)	0.22315 (+A(−0.50386) cos[(m/n + 3/(4n)) P2])	[m/n+3/(4n)]	0.93010 (+A(0.86379) cos[(m/n + 3/(4n)) P2])
S	P(1/−c)	0.27685 (−A(0.12823) cos[(m/n + 1/(4n)) P1])	[m/n+1/(4n)]	0.069900 (−A(−0.99174) cos[(m/n + 1/(4n)) P1])
S	P(1/−c)	0.078900 (−A(−0.14184) cos[(m/n + 1/(4n)) P1])	[m/n+1/(4n)]	0.053810 (−A(−0.98989) cos[(m/n + 1/(4n)) P1])
S	P(1/−c)	0.082350 (−A(−0.54548) cos[(m/n + 1/(4n)) P1])	[m/n+1/(4n)]	0.94390 (−A(0.83812) cos[(m/n + 1/(4n)) P1])
S	O(2/+c)	0.21040 (+A(−0.14961) cos[(m/n + 3/(4n)) P2])	[m/n+3/(4n)]	0.17021 (+A(−0.98874) cos[(m/n + 3/(4n)) P2])
S	O(2/+c)	0.39790 (+A(0.10008) cos[(m/n + 3/(4n)) P2])	[m/n+3/(4n)]	0.30290 (+A(−0.99498) cos[(m/n + 3/(4n)) P2])
S	O(2/+c)	0.41090 (+A(0.10419) cos[(m/n + 3/(4n)) P2])	[m/n+3/(4n)]	0.20531 (+A(−0.99456) cos[(m/n + 3/(4n)) P2])
S	O(1/+c)	0.58910 (+A(0.48273) cos[(m/n + 1/(4n)) P1])	[m/n+1/(4n)]	0.79469 (+A(0.87577) cos[(m/n + 1/(4n)) P1])
S	O(1/+c)	0.60210 (+A(0.54599) cos[(m/n + 1/(4n)) P1])	[m/n+1/(4n)]	0.69710 (+A(0.83779) cos[(m/n + 1/(4n)) P1])
S	O(1/+c)	0.78960 (+A(0.61425) cos[(m/n + 1/(4n)) P1])	[m/n+1/(4n)]	0.82979 (+A(0.78911) cos[(m/n + 1/(4n)) P1])
S	P(2/−c)	0.91765 (−A(0.96789) cos[(m/n + 3/(4n)) P2])	[m/n+3/(4n)]	0.056100 (−A(−0.25136) cos[(m/n + 3/(4n)) P2])
S	P(2/−c)	0.92110 (−A(0.63622) cos[(m/n + 3/(4n)) P2])	[m/n+3/(4n)]	0.94619 (−A(0.77151) cos[(m/n + 3/(4n)) P2])
S	P(2/−c)	0.72315 (−A(0.49345) cos[(m/n + 3/(4n)) P2])	[m/n+3/(4n)]	0.93010 (−A(0.86977) cos[(m/n + 3/(4n)) P2])
S	P(1/+c)	0.77685 (+A(0.94814) cos[(m/n + 1/(4n)) P1])	[m/n+1/(4n)]	0.069900 (+A(−0.31786) cos[(m/n + 1/(4n)) P1])
S	P(1/+c)	0.57890 (+A(0.88361) cos[(m/n + 1/(4n)) P1])	[m/n+1/(4n)]	0.053810 (+A(−0.46822) cos[(m/n + 1/(4n)) P1])
S	P(1/+c)	0.58235 (+A(0.53999) cos[(m/n + 1/(4n)) P1])	[m/n+1/(4n)]	0.94390 (+A(0.84167) cos[(m/n + 1/(4n)) P1])
S	O(2/−c)	0.71040 (−A(0.88057) cos[(m/n + 3/(4n)) P2])	[m/n+3/(4n)]	0.17021 (−A(−0.47392) cos[(m/n + 3/(4n)) P2])
S	O(2/−c)	0.89790 (−A(0.97541) cos[(m/n + 3/(4n)) P2])	[m/n+3/(4n)]	0.30290 (−A(−0.22041) cos[(m/n + 3/(4n)) P2])
S	O(2/−c)	0.91090 (−A(0.94376) cos[(m/n + 3/(4n)) P2])	[m/n+3/(4n)]	0.20531 (−A(−0.33062) cos[(m/n + 3/(4n)) P2])

image shown here). The reason for the absence of the $\vec{q}_1$ satellites in the DPs is either sample heating above the $\vec{q}_1$ onset temperature T_1 by electron irradiation, or a variation in stoichiometry, which possibly influences the formation and onset temperature of the $\vec{q}_1$ CDW. It should be pointed out that recent linear and nonlinear transport studies revealed samples showing only the T_2 transition, without any evidence of the T_1 transition [30,31]. In accord with the doubled modulation unit cell along the $\vec{a}_0$ direction, the IFFT image formed with satellites only [bottom region of Fig. 2(b)] shows areas with strong and weak CDW modulation pattern and with a phase shift of π between adjacent layers. The areas with a less pronounced modulation pattern are a result of beating interference between the slightly different modulation pattern periods of the two CDWs. However, the modulation pattern does not vanish completely as the $\vec{q}_1$ satellites have much weaker intensity in comparison to the $\vec{q}_2$ satellites.

C. Low-temperature scanning tunneling microscopy

Since HR HAADF-STEM images of the [100] zone failed to give proper information for structural modeling, LT STM was employed to study the structure of the (100) VdW surface of NbS_3-II. The method is convenient in this particular case, because it largely excludes contributions from subsurface planar defects. An LT STM image of a freshly cleaved (100) VdW surface is shown in Fig. 4(a). In addition to the regular periodicity formed by four pairs of columns, three isosceles (type-I or O-orange, type-III or Y-yellow and type-IV or P-purple) and one almost equilateral (type-II or R-red), the image also reveals one longer period along the $\vec{c}_0$ direction, representing a stacking fault (labeled as SF). Similarly, shorter periods were also observed. The basic structure unit cell and its simulated STM image [32] are overlaid in Fig. 3 onto an enlarged section of the experimental STM image. It is clearly shown in Figs. 3 and 4(a) that the atoms belonging to the brightest Y columns are out-of-phase with those belonging to the O and P columns. These phase shifts are also in clear accord with the overlaid atomic model and with the arrangement of the bicapped NbS_3 columns as shown in Fig. 3. Therefore the four different pairs of columns can be clearly distinguished.

Regarding CDWs, it is obvious that from the four pairs of columns only two, the O and P ones are clearly modulated. Of those, the left-handed P columns are slightly brighter than the right-handed O columns. These two column types also appear much brighter than the unmodulated R column, while the brightest Y columns show no clearly detectable modulation. The modulations of adjacent O and P columns are always in-phase.

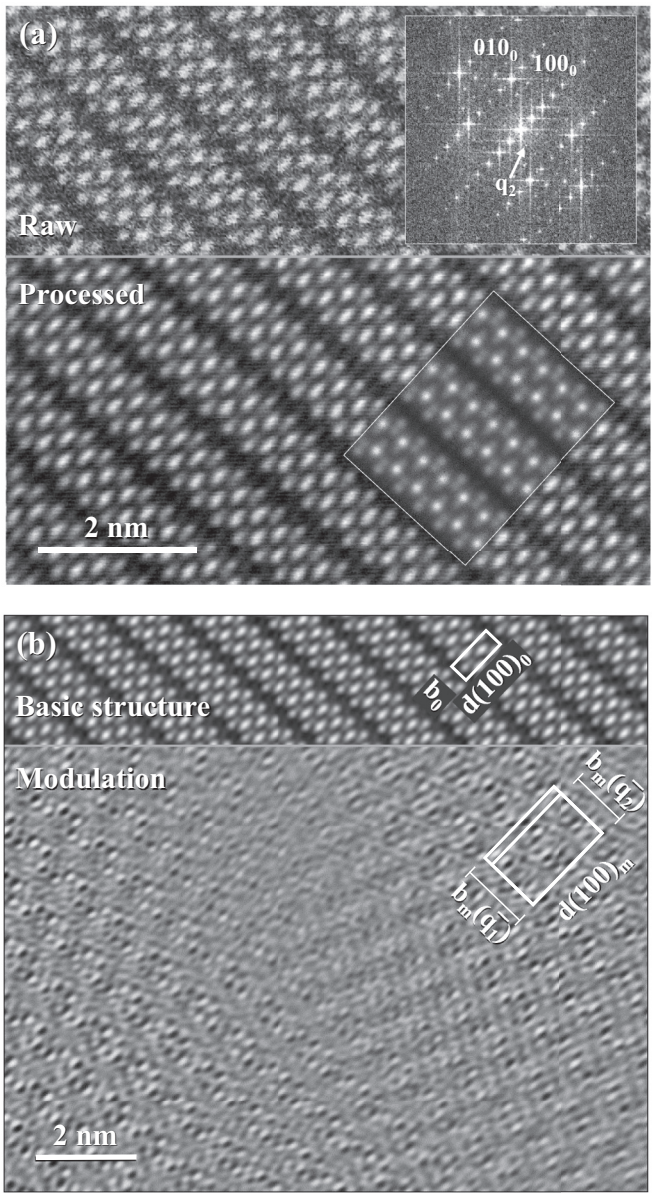

FIG. 2. (a) Raw (upper region) and processed (bottom region) HAADF-STEM image of NbS_3-II, viewed along the [001] direction. The corresponding FFT image is shown in the upper right inset. The calculated HAADF-STEM image of the structural model is shown overlaid in the inset at the lower right. (b) IFFT images formed separately with the strong basic structure reflections (upper narrow region) and with the weak IC satellites (wider bottom region). The projected unit cells of the basic structure and both CDW modulation patterns are outlined. Note that there is a phase shift of π between the CDW modes along adjacent layers.

Although the modulated columns show at certain places a variation in intensity along and between the columns, it cannot be clearly determined from the STM image whether the two columns forming a surface-subsurface pair (O-P and P-O) are modulated by the same or by two different CDWs. The arrangement of the columns and the possible G_Ms, determined in accord with the corresponding electron DPs, allow both possibilities. The FFT of the STM image in Fig. 4(b) and the corresponding IFFT in Fig. 4(c), obtained with the IC

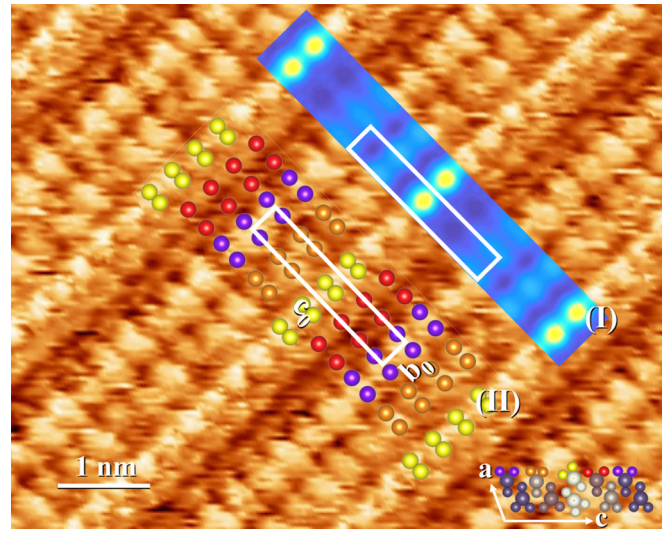

FIG. 3. An enlarged area of Fig. 4(a) with an overlaid basic structure model and its corresponding simulated STM image, both with outlined unit cells. Different types of columns are marked by the same colors as in Fig. 1. In the projection of the calculated model structure, only the topmost S atoms of each column are shown (see the bottom-right inset).

satellites only, prove that both IC CDWs, though detected with different intensities in the FFT, are indeed present. It implies that either the amplitudes of the two CDWs or their occupancy must be different. All these observations are similar to what was more clearly observed in $NbSe_3$ [13,15], where it was shown that the actual modulation pattern units consisted of coupled $\vec{q}_1$ and $\vec{q}_2$ modes along pairs of symmetry-related TP columns with isosceles bases. These observations also suggest that the $\vec{q}_1$ modes, often absent in the electron DPs, are in fact present, but are (contrary to the $\vec{q}_2$ modes) disordered along the columns above the T_1 onset temperature. This is in accord with the work of He and Zhang [33], who concluded on basis of their transport measurements that the CDW transition in $NbSe_3$ takes place over a wider temperature range. However, the behavior in $NbSe_3$ and NbS_3-II show an important difference. While the IC components of the two $\vec{q}$ vectors in $NbSe_3$ add as $2(q_{1_b} + q_{2_b}) \approx 1$, those in NbS_3-II add either as $q_{1_b} + q_{2_b} = 0.650 \approx 2/3$ or as $q_{1_b} + 2q_{2_b} = 1.002 \approx 1$. Although the experimental $\vec{q}$-vector values cannot be determined with high accuracy from the electron DPs, they appear in much better accord with the second relation.

Another feature revealed in the LT STM image is the varying phase shift between CDWs along equivalent O and P columns of adjacent unit cells along the $\vec{c}_0$ direction. These vary from being in-phase to practically out-of-phase. This arbitrary phase shifts can account for the progressive weakening and streaking of the IC satellites in the electron DPs on approaching the [100] zone axis. The origin for this disorder could be the relatively large transversal distances (and consequently weaker coupling) between the CDWs and/or a frequent interchanging of the related $\vec{q}_1$ and $\vec{q}_2$ modes. The STM image also suggests that the CDW ordering is restricted to several unit cells at most along the $\vec{c}_0$ direction.

Finally, in analogy to $NbSe_3$, the R columns in NbS_3-II appear unmodulated by CDW. In contrast, the brightest Y

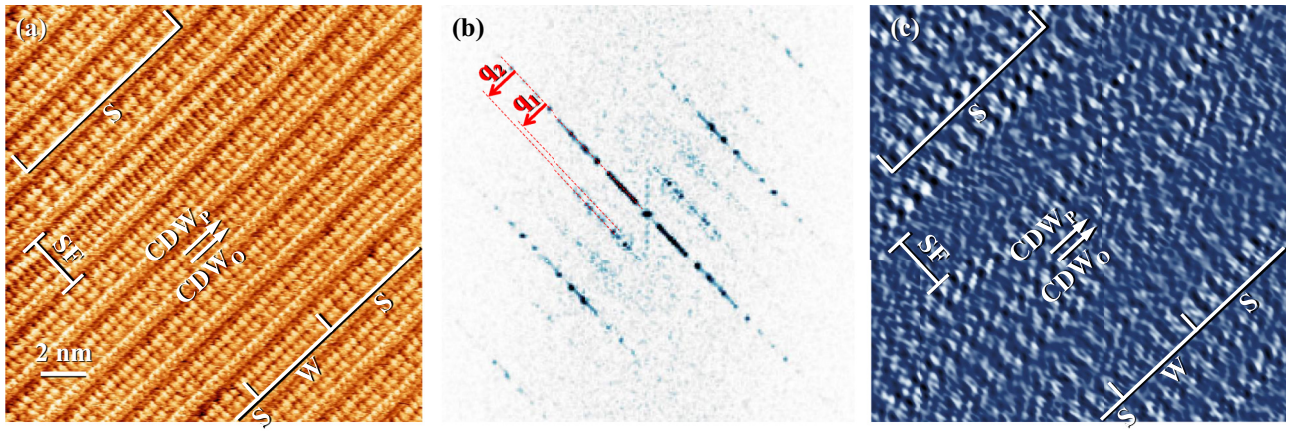

FIG. 4. (a) A $18.5 \times 18.5\,\mathrm{nm}^2$ constant current STM image of the (100) Van der Waals surface of NbS_3-II, with resolved surface S columns along the $\vec{b}_0$ direction. Note the in-phase modulations along the S chains, belonging to adjacent O and P columns, as well as strongly (S) and weakly (W) modulated sections along certain columns. (b) FFT of the STM image shown in (a). (c) The corresponding IFFT, obtained with the IC satellites only. The position of the stacking fault (SF) is indicated as a marker. Note the variation of the modulation along and between particular modulated O and P columns. Imaging parameters: $U_{\text{sample bias}} = -1.02$ V, $I_{\text{tunneling}} = 282$ pA, and $T = 140$ K.

columns, which protrude into the VdW gaps, are clearly modulated in $NbSe_3$ while no modulation was observed in NbS_3-II.

D. *Ab initio* calculation of the basic structure

It is known [34,35] that the DFT method, if applied to layered structures like NbS_3-II, allows an unrealistic extension of the structure into the VdW gap. Consequently, all relaxations were initially performed with locked $b_0 : a_0$ and $c_0 : b_0$ ratios. In all cases considered, the value of b_0 (0.3365 nm) was chosen as half of the value determined by Rijnsdorp and Jellinek [4] for NbS_3-I, while the corresponding approximate parameters a_0 and c_0 were estimated from HAADF-STEM and STM experiments. The refinements require that the angle β be finally optimized by varying a_0 as a function of β_0 with all remaining parameters kept constant. From all models considered, only the accepted one was found to be in accord with both STM and HAADF-STEM images. A XRD Le Bail fitting of the powder diagrams confirmed the chosen model was in fact in accord with the lattice parameters, reported previously by Van Smaalen [29]. A second *ab initio* refinement of the structural model using transformed Van Smaalen's parameters ($a_0 = 0.9654$ nm, $b_0 = 0.3346$ nm, $c_0 = 1.9855$ nm, and $\beta_0 = 110.71^\circ$) gave the final atomic positions. The structure of the best fitting model is shown in Fig. 1. The corresponding structural data were additionally improved by a Rietveld refinement and are collected in Table I.

E. Rietveld refinement of the basic structure

A Rietveld refinement was performed against the XRD data and is shown in Fig. 5. The refinement started with data obtained by *ab initio* calculations and resulted in an acceptable weighted profile R factor (Rwp) of 5.75% and a goodness of fit (GOF) factor of 2.68. The resultant lattice constants are $a_0 = 0.96509(8)$ nm, $b_0 = 0.33459(2)$ nm, $c_0 = 1.9850(1)$ nm, $\beta_0 = 110.695(4)^\circ$, $Z = 8$, space group $P2_1/m$ (No.11) with all Nb and S atoms in special $2e$ positions. The refined structural parameters of the Fig. 1 model are given in Table I.

IV. CHARGE DENSITY WAVE MODULATED STRUCTURE

Because of the limited computational power, *ab initio* calculations of the modulated structures, considered as LP COM with hundreds of atoms per unit cell, were not feasible to perform. Instead, DPs of different models of the modulation patterns were simulated and compared to the experimental DPs. To include both IC $\vec{q}$ vectors, the basic structure unit cell of NbS_3-II had to be accordingly enlarged along the monoclinic b_0 axis (to coincide within acceptable errors with multiples of both IC CDW periodicities) and doubled along the $\vec{a}_0$ axis (to comply with the extinction rules of the modulation pattern determined from electron DPs). Three possible

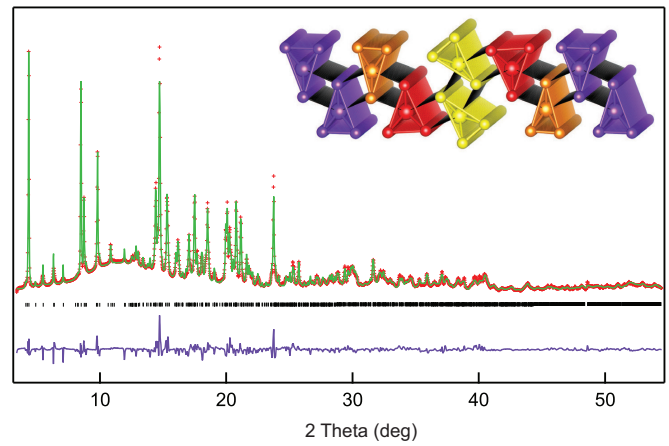

FIG. 5. Rietveld refinement of a NbS_3-II synchrotron XRD pattern, collected at 300 K. The red crosses and the green and purple lines represent the observed pattern, the calculated profile and the difference between the observed and the calculated intensities, respectively. The Bragg peaks are shown as black tick marks. The inset shows a three-dimensional model of the structure.

combinations of q_{1_b}/nb_0 and q_{2_b}/nb_0 were considered: ($2a_0$, nb_0, c_0, β) with $n = 17,\ 36$, and 37, corresponding to $q_{1_b} = 5/17,\ 11/36$, and 11/37 and $q_{2_b} = 6/17,\ 13/36$, and 13/37, respectively. The first set of ratios was suggested long ago [6] as the simplest possibility, requiring the smallest enlargement of the modulated structure unit cell. The second pair of IC components is in accord with the relation $q_{1_b} + q_{2_b} \approx 2/3$, while the third case considered ($q_{1_b} = 11/37 = 0.2973$ and $q_{2_b} = 13/37 = 0.3514$) is in best accord with the experimentally determined values of the two $\vec{q}$-vectors, i.e., $0.298b_0^*$ and $0.352b_0^*$ [2], and also in excellent accord with the alternative possibility, which requires that $q_{1_b} + 2q_{2_b} \approx 1$. The enlarged cells contain in the three cases altogether 1088 (272 Nb and 816 S), 2304 (576 Nb and 1728 S), and 2368 (592 Nb and 1776 S) atoms, respectively. These combinations were chosen to verify the positions and the appearance/disappearance of the weak IC satellites in the calculated DPs, particularly those recorded along the most important [100] and [001] zone axes.

It is noted that the approach described above is not the equivalent of a full structural analysis of the overall modulated structure employing a superspace description, which would include a refinement of all atomic positions. However, this is not possible without knowledge of the exact positions and the corresponding intensities of all reflections in the reciprocal space. As demonstrated below, analysis based on STM and simulated DPs can discriminate and restrict plausible structural models for the NbS_3-II CDW modulation.

As clearly revealed by STM experiments, the two $\vec{q}$ vectors in NbS_3-II appear only along the O and the P surface pairs of columns. The R columns are not modulated, possibly because they are more "equilateral-like," or because they are spatially separated. Although the O columns are spatially separated like the R columns are, they can be modulated by forming surface-subsurface pairs with one of two very similar P columns, inserted between the O pairs, which are also modulated. The two $\vec{q}$ vectors should be formed in accord with their expected frequency of occurrence along two adjacent (the same or very similar) columns. The very different intensities of both IC satellites suggest that the two columns forming a surface-subsurface pair (O+P) are partly modulated by $\vec{q}_2$ modes only and partly by the $\vec{q}_1/\vec{q}_2$ pairs. The resulting CDW modulated LP units evolve into temperature dependent modulated structures due to their ordered or disordered arrangements.

Pairs of CDWs must be ordered not only in accord with the extinction rules of the possible G_Ms, as determined by electron diffraction experiments [11], but also in accord with the STM images. Possible monoclinic groups, which show the same extinction rules in electron DPs, are $C2$ (No. 5), Cm (No. 8), Cc (No. 9), $C2/m$ (No. 12), and $C2/c$ (No. 15). From these five, two appear in accord with the possible ordering of the modes detected along the O and P surface columns in the corresponding STM images of the (100) VdW surfaces. If all four (two O and two P) columns are modulated by the same $\vec{q}_2$ mode, the symmetry corresponds to the space group $C2/m$ (equivalent special positions 4i). Contrary, if the subsurface two columns of the four are alternatively modulated by the $\vec{q}_1$ mode, the symmetry will be reduced into Cm (equivalent positions 2a). These two cases cannot be distinguished by STM because in both cases the surface O and P adjacent column pairs will be modulated by the same $\vec{q}_2$ modes. The higher symmetry group $C2/m$ could in fact be retained also in case the O-P surface-subsurface pairs of columns were alternatively modulated by the $\vec{q}_1$ and $\vec{q}_2$ modes. However, this would require that also both surface O and P adjacent columns were alternatively modulated by $\vec{q}_1$ and $\vec{q}_2$ CDWs. While such an ordering cannot be ruled out on theoretical grounds, it was not observed in the present STM images. Finally, if both kinds of modulated structures were formed statistically, either randomly or by forming nanodomains, the DPs will appear the same.

Only half of all Nb and S atoms (i.e., eight columns with 17, 36, or 37 Nb and three times as many S atoms each dependent on the q_{1_b}/nb_0 and q_{2_b}/nb_0 values chosen) will be modulated by $\vec{q}_1$ and $\vec{q}_2$ or by $\vec{q}_2$ modes only, while all remaining Nb and S atoms in the R and Y columns will not be displaced from their basic structure positions. Since the intensities of all IC satellites in the DPs are very weak, the corresponding modulation amplitudes must also be very small. Although the intensities cannot be accurately determined from electron DPs, it can be speculated that the actual modulation is rather confined to the lighter S instead of the heavier Nb atoms. This is also supported by the fact, clearly demonstrated during modeling, that the best agreement between experimental and calculated DPs is obtained for transversal displacements, perpendicular to the $\vec{b}_0$ direction. Thus, the only reasonable solution are "breathing modes," formed of S atoms and leaving all Nb atoms in their equilibrium positions. The corresponding modulation amplitudes are thus confined to displacements along the (010) planes, while the phase shifts between the columns are restricted by the symmetry operations of the possible G_Ms, as determined from electron DPs and STM images. One of the two possible arrangements for the case with both CDW modes present is shown in Fig. 6 with different modulated columns shown with the same colors as the corresponding columns in Fig. 1. A second possible modulation pattern unit cell is obtained by interchanging the $\vec{q}_1$ and $\vec{q}_2$ modes, i.e., by simply interchanging all P1 and P2 values, which will leave all symmetry operations of the space group Cm unchanged. After the required enlargement of the basic structure unit cell, the (x_0, y_0, z_0) coordinates of the S atoms belonging to the O and the P columns are replaced by (x, y, z) coordinates, in accord with the modulation scheme in Table II. Again, to obtain the second possible arrangement, all $\vec{q}_1$ and $\vec{q}_2$ modes (i.e., all P1 and P2 values) in Table III should be simply interchanged. The symmetry of the overall modulated structure will in both cases be $P1$ (No. 1). Finally, if only one of the two CDWs (i.e., $\vec{q}_2$) is present, all P1 values should be replaced by the P2 ones. As a result, the arrangement of the $\vec{q}_2$ modes will belong to the G_M $C2/m$ and the symmetry of the overall modulated structure will increase to $P\bar{1}$ (No. 2).

The simulated DPs show that from the three sets of ratios considered, only the two with 11 and 13 modulation periods per $36b_0$ and $37b_0$ give correct and almost identical results. They differ only in how accurate the IC satellites are positioned with regard to the strong basic structure reflections. If instead of both modes ($\vec{q}_1$ and $\vec{q}_2$) only one ($\vec{q}_2$) is present, the corresponding calculated DPs show IC $\vec{q}_2$ singlets instead of the $\vec{q}_1/\vec{q}_2$ doublets. Best fits with the experimentally observed DPs [7,11] are obtained for a rel-

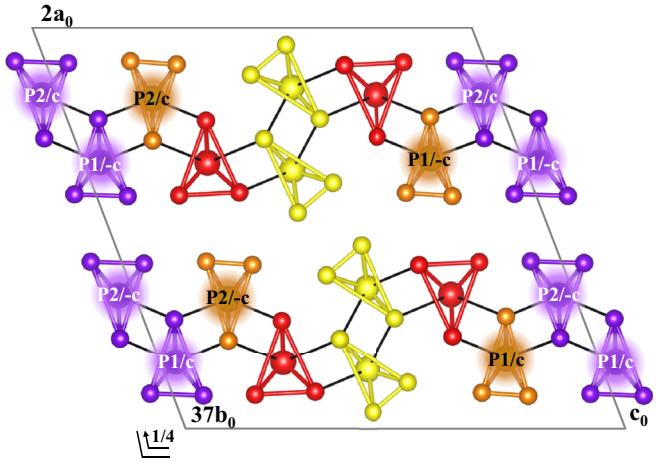

FIG. 6. The Cm modulation unit cell of NbS_3-II with one of the two possible arrangements with both, the $\vec{q}_1$ and $\vec{q}_2$ modes present. Nb and S atoms are shown as in Figure 1. The modulated columns are coded by $\vec{q}$ vectors and relative phases, with −c and c standing for $-\cos$ and cos functions and P1 and P2 for the two $\vec{q}$ vectors modulating adjacent columns. The second possible arrangement is obtained by interchanging all P1 and P2 values. By replacing all P1 with the P2 values, the alternative modulation pattern unit cell is obtained, composed of $\vec{q}_2$ modes only and corresponding to the $C2/m$ G_M.

atively small modulation amplitude A. With the breathing mode, performed by transversely displaced S atoms along the O ($\vec{q}_1$) and the P columns ($\vec{q}_2$), or vice versa, and with the phase shifts given in Table III and in Fig. 6, only actually observed IC satellites (either singlets or doublets) appear in all low-index zones. No satellites are missing and none are superficial. The calculated DPs along the two most important zones, [001] and [100], are shown in Fig. 7 for the case with $n = 37$, which is in best accord with the experimental values. The modulation amplitudes of both modes were taken as $A = 0.0033$ in units of $2a_0$ and c_0 and multiplied by factors, dependent on the direction of the displacements with respect to the $\vec{a}_0$ and $\vec{c}_0$ axes. In the simulated DPs, the satellites are drawn proportional to the logarithms of the calculated intensities for all intensities over 0.05 of the intensity of the strongest 020 basic structure reflection, or with this fixed minimum intensity for all other weaker satellites. In addition to the extinction rules, required by the corresponding G_Ms, the intensities of all satellites but the allowed ones, are below the accuracy of the numerical calculation (less than 10^{-7} of the intensity of the 020 reflection). All satellites, allowed by the G_Ms and not present in the calculated DPs, appear in the experimental electron DPs as a result of dynamical scattering. However, given satellite amplitudes are calculated in the simulations while the observed intensities incorporate the effects of dynamical scattering, only the nature of the modulation pattern is accessible through this approach.

As in the case of $NbSe_3$, the two CDWs in NbS_3-II are not equally stable at elevated temperatures. While the $\vec{q}_2$ satellites can be observed in electron diffraction experiments during repeated cycling to above 400 K, the temperature of $\vec{q}_1$ disappearance is only slightly above room-temperature at about 360 K [6,7]. However, the ordering of the two modes

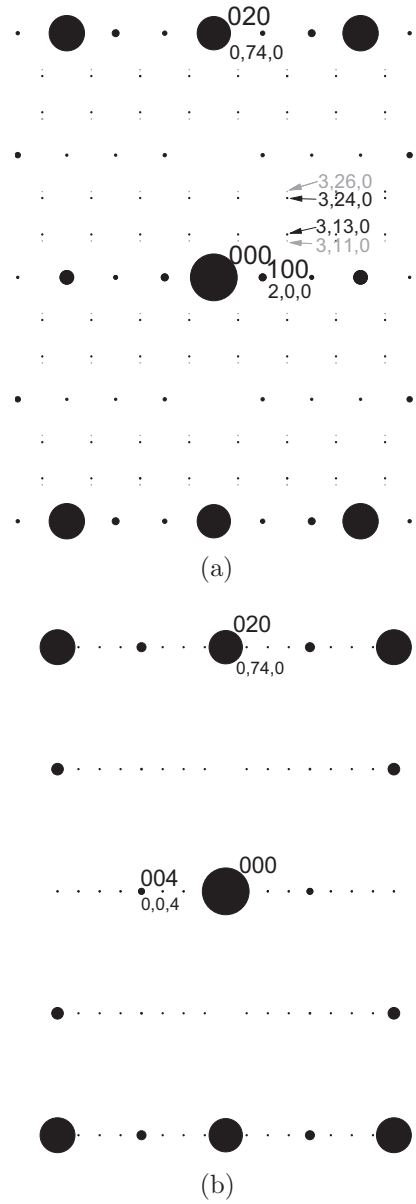

FIG. 7. Simulated DPs of NbS_3-II with the electron beam along the [001] (a) and [100] (b) zone axes for the proposed model with the two $\vec{q}$ vectors corresponding to 11 ($\vec{q}_1$) and 13 ($\vec{q}_2$) periods per $37b_0$. Large and small indices refer to the basic and the modulated structures. The $\vec{q}_1$ and $\vec{q}_2$ satellites are drawn gray and black, respectively.

in NbS_3-II is different from the one in $NbSe_3$ [11], where they form different modulation unit cells, one primitive and the other centered. As a result, for $NbSe_3$, the corresponding satellites in the electron DPs appear separated. In contrast, for NbS_3-II, both modes form equivalent centered modulation pattern cells, whose IC satellites in the DPs appear as close pairs and obey the same extinction rules.

In the case where adjacent pairs of columns are alternatively modulated by $\vec{q}_1$ and $\vec{q}_2$, the two outer O and the two inner P columns of the group of four columns (i.e., O-P-P-O) will be modulated in accord with Fig. 6. Since both modes are IC with respect to the basic structure and to one another, they will also be ordered or disordered independently. The $\vec{q}_1$

satellites are generally much weaker than the $\vec{q}_2$ satellites at all temperatures, indicating that either the modulation amplitudes or the frequency of appearance of both modes are very different. Since both $\vec{q}_1$ and $\vec{q}_2$ modes can occupy either O or P columns, which are also structurally alike, and their onset temperatures relatively close, we expect both modulation amplitudes to be similar. Therefore it is most likely that the frequency of appearance of both modes are different and the transversal ordering of the $\vec{q}_2$ modes will accordingly remain stable to higher temperatures, while the $\vec{q}_1$ modes, although present, will become disordered and will give no detectable contribution to the DPs [7,33].

The hk0 satellites of the overall LP modulated structure, present in the [001] zone, are all allowed in both possible corresponding space groups $P1$ and $P\bar{1}$. However, the appearance of the satellites must also comply with the convolution determined by both possible G_Ms, which require that $h_m + k_m =$ even. Both modes, with only the S atoms modulated transversally, are presumed to be harmonic. Thus, only first-order satellites to the strongest basic structure reflections will actually appear in the DPs. In the [100] zone, the first-order pairs of satellites to the basic structure reflections will be forbidden, while the second-order ones, though allowed, will be too weak to appear. As a result, no satellites will be detected in this particular zone, in either the calculated or experimental DPs. However, weak second order satellites may appear in case the modulation is not exactly harmonic, or if the breathing mode of the S atoms is accompanied by a weak longitudinal modulation of the Nb atoms by stretching and shortening the average Nb-Nb distances. Calculations show that as long as the corresponding Nb displacements stay small, they will not influence the appearance of the simulated DPs.

It is noted that our simulation of electron DPs assumes a perfect atomic lattice of $P2_1/m$ symmetry (Table I) and a CDW modulated structure of $P1$ or $P\bar{1}$ symmetry (Table III). The observed stacking faults and CDW phase incoherence (along the $\vec{c}_0$ direction) gives rise to streaky features and intensity variation observed in experimental DPs but not in the simulated DPs.

Finally, it should be emphasized that the description of the overall simulated modulated structure by means of LP COM superstructures represented the most convenient way to study the ordering of both $\vec{q}$ vectors and to compare the models in a straightforward way with the available experimental evidence, particularly with the LT STM images. The modulated structure with both CDWs included can also be described in a mathematically more elegant way, i.e., by means of the one-line-notation of the corresponding $3+2$-dimensional SSG [8,9,36] as $P2_1/m(0.5, \vec{q}_1, 0)00(0.5, \vec{q}_2, 0)00$, which corresponds in the standard setting with $\vec{c}_0$ the direction of both CDW modes, to $P2_1/m(0, 0, \vec{q}_1)00(0, 0, \vec{q}_2)00$ $(No.11.2.5.3)$.

V. DISCUSSION

The basic structure space group of the NbS_3-II was determined previously [11], without any knowledge of the arrangement of atoms in the corresponding unit cell. The current *ab initio* calculations and the Rietvelt XRD refinement show that all four pairs of columns are different, with three of the four being clearly isosceles and the last more equilateral-like. The symmetry related pairs of the equilateral-like R and the clearly isosceles O columns are spatially separated, while the remaining Y and P isosceles columns appear as adjacent pairs. All structural models of the basic structure considered belonged to the space group $P2_1/m$. From the different possible solutions regarding the symmetry related pairs of the four column types, only the proposed model was found to be consistent with the available experimental evidence and with the *ab initio* calculations. This basic structure of NbS_3-II differs from that of $NbSe_3$ practically only in the presence of an additional P pair of isosceles columns, inserted between the slightly different O columns.

The observed relationship of the IC components of the two $\vec{q}$ vectors, which add to a COM value as $q_{1_b} + 2q_{2_b} \approx 1$ could occur only by chance. However, this appears unlikely given the observation of similar relationships for several other related 1D MX_3 compounds with two concurrent IC CDWs. Thus the NbS_3-II CDW might be considered as a kind of composite CDW modulation.

In the present model, the two $\vec{q}$ vectors are directed along the TP columns, with only their IC y components different from zero. Both modes are also ordered in exactly the same way and they obey the same extinction rules in the corresponding DPs. It should be pointed out that the two IC satellites forming $\vec{q}_2$ and $\vec{q}_1$ pairs in the electron DPs may be taken as first- and second-order reflections. However, the extinction rules of the possible G_Ms contradict such a possibility. There is no space group that would allow higher-order satellites only along lines midway between the strong basic structure reflections. This clear coupling of both CDWs in NbS_3-II is not only in accord with the STM and HAADF-STEM images, but may suggest that CDW sliding is a result of an easy switching between the two coupled IC modes [13].

The clear doubling of the modulation pattern unit cell is in accord with the space group $C2/m$, determined long ago on the basis of electron diffraction experiments only [11]. However, the same extinction rules are obeyed by a few further space groups. The STM images reveal that pairs of O and P surface columns are modulated by the same CDW mode and are ordered in-phase. The actual symmetry of the modulation pattern can correspond to the space group $C2/m$ only if all four columns (i.e., both O and P pairs) are modulated by the same $\vec{q}_2$ modes. The same symmetry would apply if these were $\vec{q}_1$ modes instead of the $\vec{q}_2$ ones. If to the contrary, the adjacent pairs of top-bottom columns are alternatively modulated by the $\vec{q}_1$ and $\vec{q}_2$ modes, the symmetry of the G_M is reduced into Cm. Consequently, both G_M groups, $C2/m$ and Cm are in accord with electron diffraction and with STM experiments. There is no direct experimental evidence available to show which of the two possible arrangements of the two modes will actually appear more frequently. The frequency of appearance of both modes can only be inferred from the observed differences in intensity of the corresponding satellites. If both possibilities, the first with $\vec{q}_2$ modes only and the second with both modes alternatively occupying adjacent O an P columns, appear on average with the same likelihood, the $\vec{q}_2$ contribution to the DPs will exceed that of $\vec{q}_1$ modes. As in case of $NbSe_3$ where the two modes were suggested to interchange easily and are thus believed to be

the origin of the peculiar twinkling domains first observed in selected-area dark-field TEM images of $NbSe_3$ [37], a similar frequent interchanging of both modes may be involved in the sliding mechanism of the CDWs [13] in all 1D compounds with two IC CDWs formed along adjacent pairs of columns.

Regardless of whether both ($\vec{q}_1$ and $\vec{q}_2$) or only one ($\vec{q}_2$) of the two IC satellites are present in the electron DPs, these are, as a rule, detected as weak, but relatively sharp reflections only in DPs recorded along the [001] zone axis [6,11]. By rotating the crystal around the $\vec{b}_0$ axis away from the [001] zone, the satellites become weaker and more elongated, finally becoming undetectable at RT in the [100] zone axis orientation. This is in accord with the calculated DPs, where the intensities of the IC satellites become negligible as compared to those in the [001] zone. The atypical periods, often observed in LT STM images of the (100) VdW planes, in addition to the regular periodicity with eight columns per c_0, are likely related to intersections of the surface plane with planar faults. Since the VdW gaps between the S-Nb-S sandwiches are corrugated and with the columns remaining equidistant across the gaps, the aperiodic regions likely represent intersections of the (100) plane with (001) planar stacking faults.

The CDW modulated structure of $NbSe_3$ has previously been the subject of a detailed investigation using synchrotron radiation and a superspace description, which affords considerable insight into many aspects of the modulations present in NbS_3-II [38]. The basic structures of both compounds are closely related and the $\vec{q}$ vectors of the $\vec{q}_1$ and $\vec{q}_2$ modulations are observed to add to a commensurate value. Furthermore, in $NbSe_3$, the CDWs were shown to be supported only along a subset of the available column types, as is also suggested for NbS_3-II on the basis of the modeling of the modulation pattern employed in the present study. However, a number of important considerations exist which complicate the extension of the structural model derived for $NbSe_3$ to the case of NbS_3-II. Importantly, the LT STM studies reported here for NbS_3-II and previously for $NbSe_3$, have clearly established that different column types are involved in the modulations arising in the two compounds. While in the case of $NbSe_3$, the Y columns are uniformly strongly modulated, these columns do not support a modulation in NbS_3-II. Furthermore, the electron DPs of the modulation patterns obtained from $NbSe_3$ and NbS_3-II exhibit significant qualitative differences. While both IC $\vec{q}$ vectors in the DPs of NbS_3-II show close pairs of satellites (with the same $\vec{a}$-$\vec{c}$ bases of the $\vec{q}_1$ and $\vec{q}_2$ modulation pattern unit cells), in the case of $NbSe_3$, the satellites are widely separated (with the base of the $\vec{q}_1$ modulation pattern unit cell half smaller than the one of $\vec{q}_2$). The differences in the characteristics of the modulations may be attributable to the apparently inherent nonstoichiometry of the NbS_3 samples. NbS_3-II crystals show regularly a S deficiency of up to about 3%. In STM studies of the corrugated dichalcogenide β-$NbTe_2$, Te vacancies have been observed to form exclusively along the uppermost Te columns comprising the corrugated VdW surfaces [39]. If a similar partitioning of vacancies exists for NbS_3-II, the S deficiency could also lead to S vacancy formation along the topmost S chains of the Y columns. Since point defects locally suppress the CDWs (as, e.g., shown in TaS_2 [40]) and prevent their long-range ordering, a 3% S deficiency in NbS_3-II, if localized at the most protruded Y columns, will suppress any CDW formation, at least down to 150 K—where a weak CDW or CDW-like effect was detected in the transport properties of NbS_3-II with no corresponding evidence of any detectable structural changes [5]. If along restricted sections of the Y pairs of columns the pairwise ordering obeys the same rules and restrictions as those of the O and P columns, their contribution to the reciprocal space will coincide with the existing (already very weak) pairs of satellites. This may account for the mysterious 150 K CDW in NbS_3-II, but further solid experimental evidence is needed to draw a definitive conclusion.

VI. CONCLUSIONS

The present study offers a better understanding of the structural properties of NbS_3-II and of the entire family of MX_3 compounds in general. The basic structure of NbS_3-II is determined by combining HAADF-STEM, STM, and XRD experiments with *ab initio* calculations. It is confirmed that the basic structure unit cell of NbS_3-II is closely related to the one of $NbSe_3$, with only an additional isosceles pair of symmetry related TP columns. Only half of the columns are modulated by the two CDWs, whose IC components along the columns add to a COM value as $q_{1_b} + 2q_{2_b} \approx 1$. The ordering of the two IC CDWs is explained by considering them as an LP COM superstructure of the basic NbS_3-II structure.

ACKNOWLEDGMENTS

The work was supported by Slovenian Research Agency (ARRS) (under the Slovenia-Russia bilateral projects (BI-RU/14-15-043 and BI-RU/16-18-048) (E.Z., H.J.P.v.M., M.A.v.M., S.Š., E.T., A.P.), by the Russian Academy of Sciences (RFBR grants 16-02-01095, 17-02-01343) (V.Ya.P., S.G.Z., V.F.N., S.V.Z.-Z.), by the Ministry of Science and Technology of Taiwan (103-2923-M-002-003-MY3, 103-2112-M-002-022-MY3) (W.W.P., W.T.C.), by the AI-MAT center of National Taiwan University (NTU-107L900802), and by the Natural Science and Engineering Research Council of Canada (J.C.B.). Synthesis of the samples and some microscopic analyses were performed under the framework of RSF Grant No. 17-12-01519. The synchrotron x-ray diffraction beamtimes were awarded by National Synchrotron Radiation Research Center, Taiwan (Proposals No. S8_1507_17 and No. 2016B009-1). We thank M. W. Chu for fruitful discussion.

[1] J. Rouxel, ed., *Crystal Chemistry and Properties of Materials with Quasi-One-Dimensional Structures* (Springer, Netherlands, 1986).

[2] P. Monceau, Electronic crystals: An experimental overview, Adv. Phys. **61**, 325 (2012).

[3] M. A. Bloodgood, P. Wei, E. Aytan, K. N. Bozhilov, A. A. Balandin, and T. T. Salguero, Monoclinic structures of niobium trisulfide, APL Mater. **6**, 026602 (2018).

[4] J. Rijnsdorp and F. Jellinek, The crystal structure of niobium trisulfide NbS_3, J. Solid State Chem. **25**, 325 (1978).

[5] S. G. Zybtsev, V. Ya. Pokrovskii, V. F. Nasretdinova, S. V. Zaitsev-Zotov, V. V. Pavlovskiy, A. B. Odobesco, W. W. Pai, M.-W. Chu, Y. G. Lin, E. Zupanič, H. J. P. van Midden, S. Šturm, E. Tchernychova, A. Prodan, J. C. Bennett, I. R. Mukhamedshin, O. V. Chernysheva, A. P. Menushenkov, V. B. Loginov, B. A. Loginov, A. N. Titov, and M. Abdel-Hafiez, NbS_3: A unique quasi-one-dimensional conductor with three charge density wave transitions, Phys. Rev. B **95**, 035110 (2017).

[6] F. W. Boswell and A. Prodan, Peierls distortions in NbS_3 and $NbSe_3$, Physica B+C **99**, 361 (1980).

[7] Z. Z. Wang, P. Monceau, H. Salva, C. Roucau, L. Guemas, and A. Meerschaut, Charge-density-wave transport above room temperature in a polytype of NbS_3, Phys. Rev. B **40**, 11589 (1989).

[8] H. T. Stokes, B. J. Campbell, and S. van Smaalen, Generation of (3 + d)-dimensional superspace groups for describing the symmetry of modulated crystalline structures, Acta Crystallogr. Sect. A **67**, 45 (2011).

[9] S. van Smaalen, B. J. Campbell, and H. T. Stokes, Equivalence of superspace groups, Acta Crystallogr. Sect. A **69**, 75 (2013).

[10] S. Van Smaalen, Superspace groups and superstructures: NbS_3, Phase Transitions **16**, 169 (1989).

[11] A. Prodan, A. Budkowski, F. W. Boswell, V. Marinkov, J. C. Bennett, and J. M. Corbett, An approach to the structure of incommensurately modulated NbS_3 type II, J. Phys. C: Solid State Physics **21**, 4171 (1988).

[12] P. M. de Wolff, Dualistic interpretation of the symmetry of incommensurate structures, Acta Crystallogr. Sect. A **40**, 34 (1984).

[13] A. Prodan, H. J. P. van Midden, E. Zupanič, and R. Žitko, Nanostructured and modulated low-dimensional systems, in *Applied Crystallography XXII*, Solid State Phenomena Vol. 203-204 (Trans Tech Publications, Switzerland, 2013), pp. 42–47.

[14] A. Zettl, C. M. Jackson, A. Janossy, G. Grüner, A. Jacobsen, and A. H. Thompson, Charge density wave transition and nonlinear conductivity in NbS_3, Solid State Commun. **43**, 345 (1982).

[15] A. Prodan, H. J. P. van Midden, R. Žitko, E. Zupanič, J. C. Bennett, and H. Böhm, Charge density waves in $NbSe_3$: The models and the experimental evidence, Solid State Commun. **150**, 2134 (2010).

[16] S. G. Zybtsev, V. Ya. Pokrovskii, V. F. Nasretdinova, and S. V. Zaitsev-Zotov, Gigahertz-range synchronization at room temperature and other features of charge-density wave transport in the quasi-one-dimensional conductor NbS_3, Appl. Phys. Lett. **94**, 152112 (2009).

[17] In analogy with the dualistic notation of De Wolf [12].

[18] In Figs. 8 and 10 of Ref. [5] and in Ref. [31], there has been a mistake in the temperature scale. The correct temperature in centigrade is obtained by dividing the old T by 1.6–1.7.

[19] S. G. Zybtsev, V. Ya. Pokrovskii, V. F. Nasretdinova, and S. V. Zaitsev-Zotov, Growth, crystal structure and transport properties of quasi-one-dimensional conductors NbS_3, Physica B: Condens. Matter **407**, 1696 (2012).

[20] Except for an occasional and very weak detection in nuclear magnetic resonance (NMR) and x-ray absorption near edge structure (XANES) experiments [5].

[21] R. Kilaas, Optimal and near-optimal filters in high-resolution electron microscopy, J. Microsc. **190**, 45 (1998).

[22] C. Koch, Determination of core structure periodicity and density along dislocations, Ph.D. thesis, Arizona State University, 2002.

[23] Germany Bruker AXS, Karlsruhe, TOPASV4: General profile and structure analysis software for powder diffraction data, User's Manual (2008).

[24] P. Giannozzi, S. Baroni, N. Bonini, M. Calandra, R. Car, C. Cavazzoni, D. Ceresoli, G. L. Chiarotti, M. Cococcioni, I. Dabo, A. Dal Corso, S. de Gironcoli, S. Fabris, G. Fratesi, R. Gebauer, U. Gerstmann, C. Gougoussis, A. Kokalj, M. Lazzeri, L. Martin-Samos, N. Marzari, F. Mauri, R. Mazzarello, S. Paolini, A. Pasquarello, L. Paulatto, C. Sbraccia, S. Scandolo, G. Sclauzero, A. P. Seitsonen, A. Smogunov, P. Umari, and R. M. Wentzcovitch, Quantum espresso: A modular and open-source software project for quantum simulations of materials, J. Phys.: Condens. Matter **21**, 395502 (2009).

[25] K. F. Garrity, J. W. Bennett, K. M. Rabe, and D. Vanderbilt, Pseudopotentials for high-throughput DFT calculations, Comput. Mater. Sci. **81**, 446 (2014).

[26] J. P. Perdew, K. Burke, and M. Ernzerhof, Generalized Gradient Approximation Made Simple, Phys. Rev. Lett. **77**, 3865 (1996).

[27] F. Kadijk and F. Jellinek, The system niobium-sulfur, J. Less-Common Met. **19**, 421 (1969).

[28] S. Kikkawa, N. Ogawa, M. Koizumi, and Y. Onuki, High-pressure syntheses of TaS_3, NbS_3, $TaSe_3$, and $NbSe_3$ with $NbSe_3$-type crystal structure, J. Solid State Chem. **41**, 315 (1982).

[29] S. van Smaalen (private communication).

[30] S. G. Zybtsev, V. Ya. Pokrovskii, V. F. Nasretdinova, and S. V. Zaitsev-Zotov *et al.*, The anomalous features of the CDWs in the monoclinic phase of NbS_3, in *International School and Workshop on Electronic Crystals ECRYS-2017, August 21-September 2, 2017* (Cargese, France, 2017), http://lptms.u-psud.fr/ecrys2017/files/2017/09/PokrovskiiECRYS17.pdf.

[31] S. G. Zybtsev, V. Ya. Pokrovskii, V. F. Nasretdinova, S. V. Zaitsev-Zotov, V. V. Pavlovskiy, W. W. Pai, M. W. Chu, Y. G. Lin, E. Zupanič, H. J. P. van Midden, S. Šturm, E. Tchernychova, A. Prodan, J. C. Bennett, I. R. Mukhamedshin, O. V. Chernysheva, A. P. Menushenkov, and A. N. Titov, Coherent sliding of a charge density wave at 600 K and other properties of the quasi-one-dimensional compound NbS_3 (II), in *13th Russian Conference on Semiconductors, October 2-6, 2017* (Yekaterinburg, Russia, 2017).

[32] STM image simulations are based on a large supercell with some vacuum, $1 \times 39 \times 9k$-point grid, and an energy cutoff of 250 eV.

[33] H. Haifeng and Z. Dianlin, Charge Density Wave Gap Formation of $NbSe_3$ Detected by Electron Tunneling, Phys. Rev. Lett. **82**, 811 (1999).

[34] T. Bučko, S. Lebègue, J. Hafner, and J. G. Ángyán, Tkatchenko-Scheffler van der Waals correction method with and without self-consistent screening applied to solids, Phys. Rev. B **87**, 064110 (2013).

[35] F. Chiter, V. B. Nguyen, N. Tarrat, M. Benoit, H. Tang, and C. Lacaze-Dufaure, Effect of van der Waals corrections on DFT-computed metallic surface properties, Materials Research Express **3**, 046501 (2016).

[36] H. T. Stokes, D. M. Hatch, and B. J. Campbell, Isotropy software suite, iso.byu.edu.

[37] K. K. Fung and J. W. Steeds, Time-Dependent Images in Transmission Electron Microscopy Associated with the Phase Transitions of $NbSe_3$, Phys. Rev. Lett. **45**, 1696 (1980).

[38] S. van Smaalen, J. L. de Boer, A. Meetsma, H. Graafsma, H.-S. Sheu, A. Darovskikh, P. Coppens, and F. Levy, Determination of the structural distortions corresponding to the $\mathbf{q}^1$- and $\mathbf{q}^2$-type modulations in niobium triselenide $NbSe_3$, Phys. Rev. B **45**, 3103 (1992).

[39] D. Cukjati, A. Prodan, N. Jug, H. J. P. van Midden, P. Starowicz, E. Karič, S. W. Hla, H. Böhm, F. W. Boswell, and J. C. Bennett, The surface and domain structure of $NbTe_2$, J. Cryst. Growth **237-239**, 278 (2002).

[40] *Advances in the Crystallographic and Microstructural Analysis of Charge Density Wave Modulated Crystals*, edited by F. W. Boswell and J. C. Bennett, Physics and Chemistry of Materials with Low-Dimensional Structures (Springer Netherlands, 1999).